Modelling of the strength-porosity relationship in glass-ceramic foam scaffolds for bone repair

Modelling of the strength-porosity relationship in glass-ceramic foam scaffolds for bone repair

Qiang Chen[a,1], Francesco Baino[b,1,*], Silvia Spriano[b], Nicola Pugno[c,d,e], Chiara Vitale-Brovarone[b]

[a] *Laboratory of Biomechanics, School of Biological Science and Medical Engineering, Southeast University, 210096 Nanjing, P.R. China*

[b] *Institute of Materials Physics and Engineering, Applied Science and Technology Department, Politecnico di Torino, Corso Duca degli Abruzzi 24, 10129 Torino, Italy*

[c] *Department of Civil, Environmental and Mechanical Engineering, Università di Trento, Via Mesiano 77, 38123 Trento, Italy*

[d] *Centre for Materials and Microsystems, Fondazione Bruno Kessler, Via Sommarive 18, 38123 Povo (Trento), Italy*

[e] *School of Engineering and Materials Science, Queen Mary University of London, Mile End Road, London E1 4NS, UK*

[1] The first two co-authors contributed equally to the work.

*Corresponding author: F. Baino

Tel.: +39 011 564 4668

Fax: +39 011 564 4624

E-mail: francesco.baino@polito.it

Abstract

Foam-like glass-ceramic scaffolds based on three different glass compositions (45S5 Bioglass and two other experimental formulations, CEL2 and SCNA) were produced by sponge replication and characterized from the morphological, architectural and mechanical viewpoints. The relationships between porosity and compressive or tensile strength were systematically investigated and modelled, respectively, by using the theory of cellular ceramics mechanics and, for the first time, the new concept of quantum fracture mechanics. Models results are in good agreement with experimental findings, which highlights the satisfactory predictive capabilities of the presented approach. The developed models could have an interesting impact towards an ever more rational design of porous bioceramics with custom-made properties. Knowing the scaffold recommended strength for a specific surgical need, the application of the models allows to predict the corresponding porosity, which can be tailored by varying the fabrication parameters in a controlled way so that the device fulfils the desired mechanical requirements.

Keywords: Scaffold; Glass-ceramic; Strength; Cellular solids mechanics; Quantized fracture mechanics.

1. Introduction

Bioceramics constitute a subset of ceramic materials that are specially designed for the repair and reconstruction of diseased or damaged parts of the body. As reported by Dorozhkin in a valuable historical review [1], plaster of Paris (calcium sulphate) was the first experimented artificial bioceramic: ancient literature dating back to 975 AD notes that calcium sulphate was useful for setting broken bones in *ex vivo* applications and, by the end of the 19th century, orthopaedic

surgeons began to use plaster of Paris as a bone-filling substitute *in vivo*. Over the years, tens of bioceramic compositions have been tested, ranging from inert ceramics (e.g. alumina, zirconia and composites thereof) and calcium orthophosphates (due to the chemical similarity to mammalian bones and teeth) to bioactive glasses (amorphous ceramics) [2].

To date, bioceramics have been preferentially proposed for hard tissue repair covering all areas of the skeleton (e.g. healing of bone defects, fracture treatment, total joint replacement, bone augmentation, cranio-maxillofacial and orbital reconstruction, spinal surgery, dental field) [3-7], but in the last two decades their suitability for soft tissue engineering (e.g. glass fibres for muscle and nerve regeneration) has been also suggested [8,9].

Since the invention of 45S5 Bioglass® by Hench and associates in the early 1970s [10], silicate bioactive glasses have been the subject of great interest amongst bioceramics due to their unique property to form both *in vitro* and *in vivo*, when exposed to physiological fluids, a surface apatite layer having the ability to tightly bond to the surrounding bone tissue. This is a key feature, as the clinical success of an implantable biomaterial primarily requires the achievement of a stable interface with host tissue, as well as an adequate matching of the mechanical behaviour of the implant with the tissue to be replaced [11]. In order to fulfil the latter requirement, bioactive glasses are often designed into the form of three-dimensional (3-D) porous scaffolds, which act as templates supporting and directing tissue in-growth and regeneration [12,13]. In this regard, different methods have been proposed to produce glass or glass-ceramic (depending on the sintering conditions) scaffolds, including starch consolidation [14], H_2O_2 foaming [15], gel-casting [16], sponge replication [17-21], polyethylene (PE) particles burning-out [22-24], directional freeze drying [25,26] and software-guided manufacturing methods [27-29].

One of the key challenges in scaffold design is the achievement of a satisfactory balance between adequate porosity, that should allow biological fluid flow and cells migration, and mechanical strength, that should be comparable to that of cancellous bone; hence, under this perspective, the

development of porosity-strength relationships are of utmost importance in the attempt at optimizing the architectural properties of scaffolds, ideally at a pre-processing stage. Looking at the broad field of ceramic science, many mechanical property-porosity relationships for porous ceramics have been proposed over the years, as critically discussed by Pabst et al. in a valuable review [30]; as to porous bioactive glasses and bioceramics in general, however, the relevant literature is relatively scarce.

Reviewing the data from the literature, Gerhardt and Boccaccini [12] applied linear fitting and, in most cases, found an acceptable negative linear relationship between glass scaffold porosity and compressive strength (Fig. 1); however, the linear interpolation failed to hold for ultra-porous 45S5 Bioglass® scaffolds (porosity above 90 vol.%) [17] due to the onset of instability phenomena promoting the collapse of the scaffold micro-architecture. Baino et al. [23] proposed quadratic and cubic models correlating the theoretical porosity, established at the design stage, with the final pore content and compressive strength of glass-ceramic scaffolds fabricated by PE burning-out method; two-order polynomial fitting was also proposed to obtain compressive strength-porosity relationships for bioactive glass foams [21].

A linear correlation was also established between porosity and elastic modulus of glass-ceramic scaffolds using ultrasonic wave propagation [31]; a two-order polynomial Young's modulus-porosity relationship was assessed in the modelling of the mechanical properties of a face-cubic-centred scaffold microstructure [32]. Hellmich and associates modelled the non-linear relationship between porosity and elastic modulus of different porous bioceramics by applying homogenization of heterogeneous materials and micromechanics theory of porous solids [33].

Following the hierarchical structure of natural bone, Chen et al. [34,35] recently used a bottom-up approach and proposed a geometrical, general model for porous scaffolds with structural hierarchy to optimize tissue regeneration; they studied its basic mechanical constants and elastic-plastic stress-strain behaviour, showing that the mechanical properties are comparable to those of natural

bone. Tancret et al. [36] considered the porosities at both the micro- and macro-scale and presented a hierarchical model to predict the mechanical behaviour of biphasic calcium phosphate scaffolds.

It is worth mentioning that finite element methods (FEMs) have been gradually employed to study the mechanical behaviour of bone tissue engineering scaffolds [37], often in combination with advanced imaging techniques (e.g. X-ray micro-computed tomography [38,39]), by which the precise geometric model of the scaffold can be reconstructed. The method can thoroughly examine the stress-strain responses of scaffolds and the FEM-based quantitative analysis is helpful to understand the mechanical stimuli on cells and local stress distribution in the scaffolds.

In this work, foam-like scaffolds based on three different bioactive glass formulations were produced by sponge replication method and characterized from the morphological, architectural and mechanical viewpoints. The relationships between porosity and compressive or tensile strength were modelled following two different approaches, involving the application of cellular solids theory for the compressive case and, for the first time, the use of quantum fracture mechanics (QFM) concepts for the tensile one.

2. Experimental

2.1. Synthesis of the starting glasses

Three melt-derived glass formulations were used as starting materials for producing 3-D scaffolds by sponge replication method. The molar compositions of the glasses are reported in Table 1 and correspond to Hench's 45S5 Bioglass, well known in the biomedical field since the early 1970s and commercialized worldwide since 1985 [10], and CEL2 and SCNA, two experimental SiO_2-based glasses that have been originally developed and studied by Vitale-Brovarone and associates at Politecnico di Torino [18,40-43]. All glasses were prepared by melting the required quantities of

high-purity reagents (purchased from Sigma-Aldrich) in a platinum crucible in air (raw products and melting conditions are reported in Table 1). The melt was then quenched into cold water to obtain a "frit" that was later ground by using a six-ball zirconia mill, and the glass powders were eventually sieved through stainless steel sieves (Giuliani Technologies, Italy) to obtain particles with size below 32 μm to be used for scaffolds fabrication.

Besides, commercial 45S5 Bioglass® powder (NovaBone, USA) with particle size below 5 μm were used as received for making separate scaffold batches.

From now on, the two types of 45S5 Bioglass powders will be distinguished as follows: the melt-derived 45S5 Bioglass sieved below 32 μm will be referred to as BG32, whereas the commercial one will be denoted as BG5.

2.2. Scaffolds fabrication

Sponge replication was chosen for making scaffolds due to its excellent suitability to obtain porous bioceramics with trabecular architecture closely mimicking that of cancellous bone [13,17]. The processing schedule adopted in this work was extensively described elsewhere [19]. Briefly, small cubic blocks of a commercial open-cells polyurethane (PU) sponge (density of the porous polymer about 20 kg m^{-3}) were coated with glass powder by being impregnated in a water-based glass slurry (weight composition: 30% glass, 64% distilled water, 6% poly(vinyl alcohol) (PVA)). The slurry infiltrated the porous network of the polymeric templates, which were extracted from the slurry and eventually compressed (20 kPa for 1 s) in thickness along the three spatial directions in order to homogeneously remove the exceeding slurry. Scaffolds batches with different porosities were produced by varying the number of repetitions of this basic infiltration/compression cycle.

The samples were dried (first at room temperature for 3 h and then in an oven at 70 °C for 3 h) and afterwards thermally treated in order to remove the polymeric template and to sinter the inorganic

one. The sintering conditions as well as the crystalline phases developed accordingly are reported in Table 2. Therefore, it should be taken in account that, after sintering, all scaffolds were constituted by glass-ceramic materials; however, for sake of simplicity, the expressions "BG5, BG32, CEL2 and SCNA scaffolds" will be hereafter adopted, without further specifying their glass-ceramic nature.

2.3. Scaffolds characterization

2.3.1. Morphology

The scaffolds were chromium-coated, and their morphology and porous 3-D architecture were examined by scanning electron microscopy (SEM, Philips 525 M; accelerating voltage = 15 kV). The inner porous network of the scaffolds was also non-destructively investigated by micro-computed tomography (micro-CT; SkyScan 1174, Micro Photonics Inc.) in order to assess the total porosity, that will be used for the models development.

2.3.2. Mechanical strength

BG5, BG32, CEL2 and SCNA scaffolds were polished by using a SiC #320 paper to obtain samples suitable for mechanical tests. The compressive strength was evaluated by means of crushing tests (Syntech 10/D, MTS System Corp., cross-head speed = 1 mm min^{-1}); the failure stress σ_c (MPa) was obtained as

$$\sigma_c = \frac{L_c}{A_c} \tag{1}$$

wherein L_c (N) is the maximum compressive load applied during the test and A_c (mm^2) is the sample's cross-sectional area perpendicular to the load axis.

SCNA scaffolds were also tested under tensile loads; it was not possible to test the other scaffolds batches in tension due to their brittleness, which did not allowed their safe attachment to the testing fixtures. To the best of the authors' knowledge, there are no available standards or guidelines on how to prepare tensile test for bioceramic scaffolds; also, no data relevant to such a characterization were found in the literature, except for few studies on bioceramic/polymer porous composites [44,45]. In order to fill this gap, we propose a modification of the ASTM standard followed to test the adhesion of HA coatings on prosthetic substrates [46]. Before testing, each scaffold was glued to two loading fixtures (16-mm diameter steel cylinders to be then connected by metal pins to the testing machine) by using an epoxy resin (Araldite® AV 119, Ciba-Geigy), which is able to withstand a maximum stress of above 40 MPa (as declared by the manufacturer). At room temperature, the adhesive was a gel; its polymerization was achieved by a low-temperature treatment in oven (140 °C for 1 h). The failure tensile stress of the SCNA samples, σ_t (MPa), was calculated as

$$\sigma_t = \frac{L_t}{A_t} \tag{2}$$

wherein L_t (N) is the tensile failure load and A_t (mm^2) is the resistant cross-sectional area.

3. Modelling

3.1. Compressive case

The mechanical properties of porous solids, like the glass-ceramic scaffolds studied in this work, can be well modelled by using micromechanical analysis. The classical approach was first reported

by Gibson and Ashby who developed the so-called "density power law model" [47], obtained by analysing the bending and buckling mechanisms of ligaments in a regular cellular microframe. As a matter of fact, however, ligaments in open-cells porous materials may be subjected to complex mechanical loads (e.g. tension, bending, shear, torsion and their combinations); therefore, a general relationship between the normalized mechanical properties $\bar{M}$ of a porous solid and its relative density $\bar{\rho}$ (or porosity $p = 1 - \bar{\rho}$) was presented in the form:

$$\bar{M} = C\bar{\rho}^{\alpha} \tag{3}$$

wherein C and α are constants depending on the different constituent materials, structural morphologies and failure mechanisms (e.g. $\alpha = 1$ for pure tensile/compressive case and $\alpha = 1.5$ for pure bending case [47]).

Since the properties of the natural constituents of bone are not constant and often difficult to be determined [48], as they depend on many factors including composition, structure and harvesting site, the mechanical properties *M* of natural bone can be directly expressed as:

$$M = C\bar{\rho}^{\alpha} \tag{4}$$

Therefore, considering the potential application of the prepared porous scaffolds in the context of bone tissue engineering, Eq.(4) can be used to express the scaffold compressive strength-porosity relationship as:

$$\sigma_c = C(1-p)^{\alpha} \tag{5}$$

wherein the values of total porosity *p* are in the [0-1] range.

3.2. Tensile case

Unlike the compressive case, the tensile failure is caused by the instable crack propagation due to pores or connecting-pore cracks [49] (Fig. 2a). First, Eq. (4) provides the Young's modulus as:

$$E = C\left(1-p\right)^{\alpha} \tag{6}$$

wherein $\alpha = 3$ and $C = E_s$ are adopted [50]; E_s is the Young's modulus of the constituent bulk (pore-free) material [49].

The surface energy density of a porous material is expressed as [51,52]:

$$\gamma = \gamma_s e^{-\beta(1-\bar{\rho})} \tag{7}$$

wherein γ_s is the surface energy density of the constituent (bulk) material and β is a constant, which is typically between 1 to 9 for most porous structures [51].

Considering Eq.(6) for the Young's modulus and the high-porosity (above 40 vol.%) bulk modulus [53], the Poisson's ratio can be expressed as:

$$\upsilon = 0.5 - \frac{E}{6K} = 0.5 - \frac{3}{4}(1-\upsilon_s)(1-p)^2 \tag{8}$$

with $K = K_s \dfrac{2(1-2\upsilon_s)(1-p)}{3(1-\upsilon_s)}$,

wherein K_s and υ_s are bulk modulus and Poisson's ratio of the constituent bulk (pore-free) material, respectively.

Here, the irregular shapes of real pores in the scaffolds are equivalent to be elliptical [54] in the [xy] plane of the model, as observed in polished cross-sections of the scaffolds reported elsewhere [21]. Considering the largest elliptical crack or defect in the model (Fig. 2), which plays an important role in model's tensile failure, and according to the Irwin's fracture formula [55], the tensile strength of the scaffold can be obtained as:

$$\sigma_t = \Phi \sqrt{\frac{2E\gamma}{\pi(1-\upsilon^2)\left(a+g\right)}} \tag{9}$$

with

$$\Phi = \frac{\int_0^{\pi/2} \sqrt{\sin^2\varphi + \left(\frac{a}{b}\right)^2 \cos^2\varphi}\, d\varphi}{\sqrt[4]{\sin^2\varphi + \left(\frac{a}{b}\right)^2 \cos^2\varphi}},$$

wherein a and b are equivalent to minor and major axes of the elliptical hole, respectively, $a+g$ is the half length of the largest crack or defect in the minor axis direction, and g is the grain size. It is noted that g can be interpreted as the fracture quantum defined by Pugno and associates [49,56,57], and thus it can be calculated as:

$$g = 2E_s\gamma_s / \pi\sigma_s^2 \tag{10}$$

wherein σ_s is the tensile strength of the bulk material. Then, rearranging Eq.(9), we find:

$$\frac{\sigma_t}{\sigma_s} = \Phi \sqrt{\frac{e^{-\beta p}}{\left(1-\left[0.5-\frac{3}{4}(1-\upsilon_s)(1-p)^2\right]^2\right)\left(1+\frac{a}{g}\right)}}\,(1-p)^{1.5} \tag{11}$$

For porous materials, the grain volume V_g, the pore volume V_d and the total volume V_T satisfy the following relationship:

$$V_d = V_T - V_g \tag{12}$$

Then, dividing both sides of Eq.(12) by V_T and after some rearrangements, we can find:

$$V_d / V_g = p/(1-p) \tag{13}$$

The volume of pores disappears when $p \to 0$, and $V_d/V_g \to \infty$ when $p \to 1$. If we simply assume $(a/g)^3 \propto V_d/V_g$, then Eq.(11) becomes:

$$\frac{\sigma_t}{\sigma_s} = \Phi \sqrt{\frac{e^{-\beta p}}{\left(1-\left[0.5-\frac{3}{4}(1-\upsilon_s)(1-p)^2\right]^2\right)\left(1+\kappa\sqrt[3]{p/(1-p)}\right)}}\,(1-p)^{1.5} \tag{14}$$

If we consider a peculiar case, i.e. $a = b$, the ellipse becomes a circle and $\Phi = \pi / 2$. For this case, Eq.(14) is consistent with the result of oblate spheroid derived by Sack [58], who extended the Griffith's theory to 3-D configuration. Comparing Eq.(14) with the well-known result from Gibson and Ashby [47], we observe that they are different in their final form. In particular, although the power 1.5 is identical, the square-root term with respect to the porosity is not a constant and the present result includes the shape factor of pores.

4. Results and discussion

4.1. Morphological investigations

Fig. 3a shows the open-cells structure of a typical PU sponge, used as a sacrificial template for scaffolding, that exhibits a 3-D network of pores ranging from 200 up to 800 μm with strut thickness within 10-50 μm. The porosity of the sponge, assessed by weight-volume measurements, was above 90 vol.%. During the sponge replication process, the polymeric porous template was coated with a thin and continuous layer of glass particles (Fig. 3b) in order to obtain, after the appropriate high-temperature thermal treatment (Table 2), an inorganic glass-derived replica of the foam. The sintered scaffolds were glass-ceramic because the thermal treatment induced the nucleation and growth of crystalline phases (Table 2) in the glass amorphous phase, as detected elsewhere by XRD investigations [19,21,43,49].

The typical appearance of the produced cubic scaffolds is shown in Fig. 4a: the macroporous nature of the samples is already apparent in this low-magnification picture. From the architectural viewpoint, all glass-ceramic scaffolds closely mimicked the 3-D foam-like structure of cancellous bone and exhibited well-densified and sound trabeculae (Fig. 4b-d). This is an important achievement especially in the case of BG5 and BG32 scaffolds, since the poor mechanical strength

of 45S5 Bioglass® scaffolds reported in the literature (0.3-0.4 MPa) was mainly attributed to the presence of hollow struts [17]. The persistence of the "trace" of the starting PU sponge as an inward cavity along the axis of sintered scaffold struts is due to the peculiar sintering behaviour of 45S5 Bioglass®, characterized by a small sinterability window [21]. The optimization of the thermal treatment allowed to overcome this problem, thereby obtaining mechanically suitable scaffolds for bone restoration (see the section 4.2).

Micro-CT investigations (Fig. 5) revealed a good 3-D pores interconnectivity in all scaffolds batches (the open porosity was estimated to be above 90 % of the overall porosity), which is a key feature for bone tissue engineering applications. In fact, the flow of culture medium containing cells during cell seeding is critical to develop an evenly populated tissue engineering scaffold and it is fundamental that, *in vivo*, there are paths for cells to migrate, tissue to grow in and waste products to flow out. The total porosity of scaffolds significantly varied in the 35-85 vol.% range depending on the starting glass and processing parameters, such as the number of repetitions of the sponge impregnation/squeezing cycle. For instance, the SCNA scaffold shown in Figs. 5e,f clearly exhibits thicker struts and lower porosity in comparison to BG32 and CEL2 samples depicted in Figs. 5a,b and Figs. 5c,d. Micro-CT analysis further confirmed the soundness and adequate densification of the trabeculae of all scaffolds produced in this work, as already assessed by SEM investigation. An extensive characterization by micro-CT of the scaffolds have been reported elsewhere by the authors [38,39].

4.2. Mechanical properties and models results

The strengths of the four scaffolds types were studied by employing Eq.(5) and Eq.(14) for the compressive and tensile case, respectively. The fitting of the experimental data to estimate the

unknown parameters of the model was carried out by using an *ad-hoc* software code based on the least mean squares (LMS) algorithm.

The results of model fittings with the experimental compressive data are shown in Fig. 6; the model constants C and α as well as the correlation coefficient R^2 are listed in Table 3. In order to clearly contrast the two sets of 45S5 Bioglass scaffolds (BG5 and BG32) and experimental biomaterials (CEL2 and SCNA), their results are separately depicted in Fig. 6a and Fig. 6b, respectively; moreover, the global comparison between experimental findings and theoretical predictions for all scaffolds is plotted in Fig. 6c.

As to the tensile tests for SCNA scaffolds, we employed the peculiar result of Eq. (14), i.e. $a = b$. The tensile strength of the SCNA constituent (pore-free material) is 47 MPa [49] and υ_s is assumed to be 0.3; the model fitting with the experimental results is shown in Fig. 7. The fitted parameters are $\beta = 0.95$ and $\kappa = 17.36$, and the correlation coefficient R^2 equals 0.91.

Models results generally exhibit good agreements with experimental data, as demonstrated by the high values of the coefficients R^2, which also reveals the good predictive capabilities of the presented approach.

Looking at Fig. 6c, the following trend can be observed for the compressive strength of the scaffolds (under analogous porosity/architecture and manufactured by the same process):

SCNA > CEL2 > 45S5 Bioglass (BG5 and BG32)

This trend can be ascribable to intrinsic materials characteristics, and more specifically to the different mechanical features of the crystalline phases nucleated in the various glass-ceramic materials. This hypothesis can be supported by following an approach based on the fact that, in principle, materials with higher density have higher mechanical strength [21]. We observed that the

densities of $Na_2CaSi_2O_6$ (major crystalline phase of BG5 and BG32), $Na_4Ca_4(Si_6O_{18})$ (major phase of CEL2 scaffolds) and $CaSiO_3$ (found in SCNA scaffolds) are ~2.83, ~2.85 and ~2.92 g cm^{-3}, respectively, which consistently mirrors the "strength order" of the different types of scaffolds. The remarkably high strength of SCNA scaffolds can be also explained taking in account that the presence of Al_2O_3 in a glass formulation is known to increase the mechanical resistance of the material [13]; in the case of SCNA, Al_2O_3 is contained in the residual amorphous phase.

It is also interesting to compare the properties of BG5 and BG32 scaffolds (Fig. 2a), as under the same porosity the compressive strength of the former is higher than that of the latter. This can be attributable to a better coating of PU template and a higher homogeneity obtained by the very fine commercial 45S5 Bioglass® particles (size below 5 μm) with respect to non-commercial ones (size below 32 μm). Furthermore, hot-stage microscopy studies, reported elsewhere by the authors [21], revealed that compact bodies of BG32 particles undergo low densification upon heating compared to BG5 ones, which should involve the formation of "weaker" (less densified) struts in the final scaffold.

As to the tensile case for SCNA scaffolds, β does not locate in the typical 1-9 range as observed for most porous structures but is very close to the lower limit of the range; this might be caused by the relatively limited number of tested samples, whose porosity is between 42 and 65 vol.%.

Having a general look at all the four scaffolds batches, the ultimate strength in compression is between 0.2 and 27.7 MPa, thereby covering the strength range of natural cancellous bone. Indeed, it should be taken in account that the compressive strength of trabecular bone significantly varies depending on the sex, age, harvesting site and peculiar features of the patient; however, a typical 1-20 MPa range can be used as a reference [48,59]. These values also locate in the strength range of the promising hierarchical scaffold developed by Chen and co-worker [34,35], which has a multiscale structure useful for cells activities and nutrients distribution. In the case of SCNA and CEL2 scaffolds, the model powers α are 1.44 and 2.44, respectively, which are comparable to

those assessed for cancellous (1.88) and even cortical bone (1.93) [60,61]; in this regard, the two scaffolds might be particularly attractive for bone tissue engineering applications.

Focusing on SCNA scaffolds, their compressive and tensile strengths are 17.8 MPa ± 6.9 MPa and 4.9 MPa ± 1.9 MPa, respectively; just to do a rough comparison with the literature, these data are really close to those assessed for both human cancellous (1-20 MPa in compression, 10-20 MPa in tension [48,62]) and bovine spongy bone (12.4 MPa ± 3.2 MPa in compression and 7.6 ± 2.2 MPa in tension [63]).

Reviewing the existing literature, the model parameters of BG5 and BG32 scaffolds are interestingly comparable, as order of magnitude, to those describing the compressive yield strength of biomedical Ti-6Al-4V foams (pre-exponential constant = 336.69, power = 3.3) [64]; indeed, the difference of fracture mechanisms in the two cases (glass-derived scaffolds are brittle, metal foams are ductile) should be taken into account. The toughness of 45S5 Bioglass scaffolds could be increased by the incorporation of a polymeric phase in the glass or glass-ceramic matrix, thereby creating a porous composite [65].

In summary, it seems that SCNA scaffold is the most suitable biomaterial for orthopaedic applications requiring load-bearing ability of the implanted graft. However, as shown elsewhere by the authors [20], SCNA and its glass-ceramic derivatives exhibit low *in vitro* bioactivity, i.e. the hydroxyapatite (HA) formation on the biomaterial surface after contact with acellular simulated body fluids obeys very slow kinetics. Nevertheless, recent studies demonstrated that the HA formation can significantly speed up *in vivo* and osteogenesis occurs thanks to the key role played by the bone-like porous architecture of the scaffold [66].

Besides being proposed as bone fillers, SCNA scaffolds could be also suggested for more complex orthopaedic applications due to their attractive mechanical properties. For instance, a couple of previous studies indicate the possible suitability of SCNA to manufacture trabecular-like coatings on prosthetic devices with the aim to enhance the implant osteointegration [20,49]. The findings

achieved in the present study further demonstrate that SCNA scaffolds might be successfully applied also in contexts requiring high strength under tension, for instance due to multiaxial loading, which actually occurs in joint prostheses.

To the best of the authors' knowledge, a comparison between the tensile strength of SCNA scaffolds with that of other porous glasses/glass-ceramics is not possible due to the lack of experimental data reported in the existing literature: in fact, the majority of bioceramic scaffolds, such as the 45S5 Bioglass-derived samples, are too fragile to be safely handled for this test according to current standards. The development of new and even more appropriate protocols or guidelines for testing the mechanical properties of glass-derived scaffolds would be highly desirable, as a useful tool for researchers working on this topic.

4.3. Potential implications in the field of porous ceramics for healthcare

Biomaterials science, mechanical modelling of porous solids and regenerative medicine are apparently quite far disciplines, each one featured by a specific knowledge. Therefore, on one hand the dialogue amongst scientists working in these different research fields is often difficult due to the different "language" spoken by the researchers, which makes the collaboration a complex task; on the other hand, however, the cross-fertilization amongst the various abilities allows to gain more in-depth knowledge and to develop new, often unusual approaches to solve problems.

Thanks to the synergy amongst different research groups, in this work the concepts and background traditionally used to solve structural mechanics problems were applied to the biomedical field in order to model the strength-porosity relationship of different glass-ceramic foam-like scaffolds for bone repair. The obtained models can be a valuable tool at the designer's/manufacturer's disposal to link the mechanical properties of final scaffolds with the design/processing parameters, in order to optimize the biomaterial performance. For instance, in the case of sponge-replicated scaffolds – like

the samples fabricated in this work – the number of impregnation/squeezing cycles of the polymeric foam used as a sacrificial template can be varied in a controlled way to obtain a desired pore content, which plays a key role in affecting the mechanical properties of the material. Therefore, the analytical model describing the strength-porosity relationship can be successfully employed for a "predictive purpose" and not only in a "descriptive way": in fact, knowing the minimum strength (or strength range) recommended for a given biomedical application, it is possible to purposely tailor the scaffold porosity (acting on the processing cycles in a controlled fashion) so that the device can fulfil the desired mechanical requirements. The impact of the approach proposed in the present work over the design of porous bioceramics could be very significant in the near future. Ideally, the suggested method would allow to overcome the limitations and inaccuracies of the traditional "trial and error" approach to optimize the mechanical performances of bone scaffolds, also avoiding unwanted loss of experimental time used for samples preparation and testing.

Furthermore, the models can be used as a guideline for material selection. For instance, we can suppose that the restoration of a given bone defect may require a scaffold with porosity of at least 60 vol.% and compressive strength of at least 10 MPa; having a look at Fig. 6, we could exclude the use of BG5, BG32 and CEL2 scaffolds, as only SCNA samples are able to fulfil both criteria. On the other hand, it should be also taken into account that the scaffold strength can significantly increase *in vivo* due to tissue in-growth, since the cells adherent on scaffold, the newly formed tissue and the scaffold itself create a biocomposite construct *in situ*, thereby increasing the time-dependent scaffold strength and toughness [29]. In this regard, therefore, also CEL2 could be a valuable option thanks to its excellent bioactivity, even superior to that of 45S5 Bioglass [39].

In summary, it is evident that the design and fabrication of the "best" scaffold for a given application is a complex issue that often requires a compromise amongst different and opposite criteria (e.g. mechanical strength and bioactivity); the approach proposed in this work may be an

helpful tool to guide researchers towards an ever more rational design of bone tissue engineering porous biomaterials.

5. Conclusions

In this paper, 45S5 Bioglass-, CEL2- and SCNA-derived glass-ceramic scaffolds for possible use in bone tissue engineering were fabricated by the sponge replication method; the total porosity of the samples was varied in the 35-85 vol.% range by changing the processing parameters. The samples exhibited a 3-D porous architecture closely mimicking that of cancellous bone. The scaffolds were mechanically tested under compression and tension and the obtained experimental results were used to develop compressive/tensile models describing the porosity-strength relationships. From a mechanical viewpoint, the SCNA scaffold seems to be particularly suitable for bone substitution, as their ultimate compressive and tensile strengths (17.8 ± 6.9 MPa and 4.9 ± 1.9 MPa, respectively) are comparable to those assessed for bovine and human spongy bone. The models can be used in a "direct fashion" to predict the scaffold mechanical strength using the porosity as a model input, but they can be also interestingly employed in an "inverse way": using the mechanical strength as an input, the scaffold designer can obtain the corresponding porosity, which is properly tailored by setting the fabrication parameters at the manufacturing stage. Therefore, the proposed approach represents an helpful tool towards a custom-made design of porous bioceramics, in order to optimize manufacturing time and scaffold performance.

Acknowledgements

Q.C. is supported by Priority Academic Program Development of Jiangsu Higher Education Institutions (No. 1107037001).

N.P. thanks the European Research Council (ERC StG Ideas 2011 BIHSNAM and ERC Proof of Concept REPLICA2 2013) and the European Union (Graphene Flagship) for support.

This work was also partially supported by the EU-funded project MATCh ("Monoblock acetabular cup with trabecular-like coating", Grant no. 286548).

References

[1] Dorozhkin SV. A detailed history of calcium orthophosphates from 1770s till 1950. Mater Sci Eng C 2013;33:3085-110.

[2] Chevalier J, Gremillar L. Ceramics for medical applications: a picture for the next 20 years. J Eur Ceram Soc 2009;29:1245-55.

[3] Vallet-Regi M, Ruiz-Hernandez E. Bioceramics: from bone regeneration to cancer nanomedicine. Adv Mater 2011;5177-218.

[4] Baino F. Biomaterials and implants for orbital floor repair. Acta Biomater 2011;7:3248-66.

[5] Rahaman MN, Day DE, Bal BS, Fu Q, Jung SB, Bonewald LF et al.. Bioactive glass in tissue engineering, Acta Biomater 2011;7:2355-73.

[6] Jones JR. Review of bioactive glass: from Hench to hybrids. Acta Biomater 2013;9:4457-86.

[7] Dorozhkin SV. Calcium orthophosphate-based bioceramics. Materials 2013;6:3840-942.

[8] Shah R, Sinanan ACM, Knowles JC, Hunt NP, Lewis MP. Craniofacial muscle engineering using a 3-dimensional phosphate glass fibre construct. Biomaterials 2005;26:1497-505.

[9] Vitale-Brovarone C, Novajra G, Lousteau J, Milanese D, Raimondo S, Fornaro M. Phosphate glass fibres and their role in neuronal polarization and axonal growth direction. Acta Biomater 2012;8:1125-36.

[10] Hench LL. The story of Bioglass®. J Mater Sci: Mater Med 2006;17:967-78.

[11] Hench LL. Bioceramics: from concept to clinic. J Am Ceram Soc 1991;74:1487-510.

[12] Gerhardt LC, Boccaccini AR. Bioactive glass and glass-ceramic scaffolds for bone tissue engineering. Materials 2010;3:3867-910.

[13] Baino F, Vitale-Brovarone C. Three-dimensional glass-derived scaffolds for bone tissue engineering: current trends and forecasts for the future. J Biomed Mater Res A 2011;97:514-35.

[14] Vitale-Brovarone C, Di Nunzio S, Bretcanu O, Verné E. Macroporous glass-ceramic materials with bioactive properties. J Mater Sci: Mater Med 2004;15:209-17.

[15] Yuan H, De Buijin JD, Zhang X, Van Blitterswijk CA, De Groot K. Bone induction by porous glass ceramic made from Bioglass® (45S5). J Biomed Mater Res (Appl Biomater) 2001;58:270-6.

[16] Gough JE, Jones JR and Hench LL. Nodule formation and mineralization of human primary osteoblasts cultured on a porous bioactive glass scaffold. Biomaterials 2004;25:2039-46.

[17] Chen QZ, Thompson ID, Boccaccini AR. 45S5 Bioglass®-derived glass-ceramic scaffolds for bone tissue engineering. Biomaterials 2006;27:2414-25.

[18] Vitale-Brovarone C, Verné E, Robiglio L, Appendino P, Bassi F, Martinasso G et al. Development of glass-ceramic scaffolds for bone tissue engineering: characterisation, proliferation of human osteoblasts and nodule formation. Acta Biomater 2007;3:199-208.

[19] Vitale-Brovarone C, Baino F, Verné E. High strength bioactive glass-ceramic scaffolds for bone regeneration. J Mater Sci: Mater Med 2009;20:643-53.

[20] Vitale-Brovarone C, Baino F, Tallia F, Gervasio C, Verné E. Bioactive glass-derived trabecular coating: a smart solution for enhancing osteointegration of prosthetic elements. J Mater Sci: Mater Med 2012;23:2369-80.

[21] Baino F, Ferraris M, Bretcanu O, Verné E, Vitale-Brovarone C. Optimization of composition, structure and mechanical strength of bioactive 3-D glass-ceramic scaffolds for bone substitution. J Biomater Appl 2013;27:872-90.

[22] Vitale-Brovarone C, Baino F, Miola M, Mortera R, Onida B, Verné E. Glass-ceramic scaffolds containing silica mesophases for bone grafting and drug delivery. J Mater Sci: Mater Med 2009;20:809-20.

[23] Baino F, Verné E, Vitale-Brovarone C. 3-D high strength glass-ceramic scaffolds containing fluoroapatite for load-bearing bone portions replacement. Mater Sci Eng C 2009;29:2055-62.

[24] Bellucci D, Cannillo V, Sola A, Chiellini F, Gazzarri M, Migone C. Macroporous Bioglass®-derived scaffolds for bone tissue regeneration. Ceram Int 2011;37:1575-85.

[25] Fu Q, Rahaman MN, Bal BS, Brown RF. Preparation and in vitro evaluation of bioactive glass (13-93) scaffolds with oriented microstructures for repair and regeneration of load-bearing bones. J Biomed Mater Res A 2010;93:1380-90.

[26] Liu X, Rahaman MN, Fu Q. Bone regeneration in strong porous bioactive glass (13-93) scaffolds with an oriented microstructure implanted in rat calvarial defects. Acta Biomater 2013;9:4889-98.

[27] Bergmann C, Lindner M, Zhang W, Koczur K, Kirsten A, Telle R et al. 3D printing of bone substitute implants using calcium phosphate and bioactive glasses. J Eur Ceram Soc 2010;20:2563-7.

[28] Tesavibul P, Felzmann R, Gruber S, Liska R, Thompson I, Boccaccini AR et al. Processing of 45S5 Bioglass® by lithography-based additive manufacturing. Mater Lett 2012;74:81-4.

[29] Liu X, Rahaman MN, Hilmas GE, Sonny Bal B. Mechanical properties of bioactive glass (13-93) scaffolds fabricated by robotic deposition for structural bone repair. Acta Biomater 2013;9:7025-34.

[30] Pabst W, Gregorova E, Ticha G. Elasticity of porous ceramics - a critical study of modulus-porosity relations. J Eur Ceram Soc 2006;26:1085-97.

[31] Kohlhauser C, Hellmich C, Vitale-Brovarone C, Boccaccini AR, Rota A, Eberhardsteiner J. Ultrasonic characterisation of porous biomaterials across different frequencies. Strain 2009;45:34-44.

[32] Sanz-Herrera JA, Garcia-Aznar JM, Doblaré M. A mathematical model for bone tissue regeneration inside a specific type of scaffold. Biomech Model Mechanobiol 2008;7:355-66.

[33] Scheiner S, Sinibaldi R, Pichler B, Komlev V, Renghini C, Vitale-Brovarone C et al. Micromechanics of bone tissue-engineering scaffolds, based on resolution error-cleared computer tomography. Biomaterials 2009;30:2411-9.

[34] Chen Q, Huang S. Mechanical properties of a porous bioscaffold with hierarchy. Mater Lett 2013;95:89-92.

[35] Huang S, Li Z, Chen Z, Chen Q, Pugno N. Study on the elastic-plastic behavior of a porous hierarchical bioscaffold used for bone regeneration. Mater Lett 2013;112:43-6.

[36] Tancret F, Bouler JM, Chamousset J, Minois LM. Modelling the mechanical properties of microporous and macroporous biphasic calcium phosphate bioceramics. J Eur Ceram Soc 2006;26:3647-56.

[37] Lacroix D, Chateau A, Ginebra MP, Planell JA. Micro-finite element models of bone tissue-engineering scaffolds. Biomaterials 2006;27:5326-34.

[38] Renghini C, Komlev V, Fiori F, Verné E, Baino F, Vitale-Brovarone C. Micro-CT studies on 3-D bioactive glass-ceramic scaffolds for bone regeneration. Acta Biomater 2009;5:1328-37.

[39] Renghini C, Giuliani A, Mazzoni S, Brun F, Larsson E, Baino F et al. Microstructural characterization and in vitro bioactivity of porous glass-ceramic scaffolds for bone regeneration by synchrotron radiation X-ray microtomography. J Eur Ceram Soc 2013;33:1553-65.

[40] Vitale-Brovarone C, Baino F, Bretcanu O, Verné E. Foam-like scaffolds for bone tissue engineering based on a novel couple of silicate-phosphate specular glasses: synthesis and properties. J Mater Sci: Mater Med 2009;20:2197-205.

[41] Vitale-Brovarone C, Baino F, Verné E. Feasibility and tailoring of bioactive glass-ceramic scaffolds with gradient of porosity for bone grafting. J Biomater Appl 2010;24:693-712.

[42] Verné E, Ferraris S, Vitale-Brovarone C, Spriano S, Bianchi CL, Naldoni A et al. Alkaline phosphatase grafting on bioactive glasses and glass-ceramics. Acta Biomater 2010;6:229-40.

[43] Ma H, Baino F, Fiorilli S, Vitale-Brovarone C, Onida B. Al-MCM-41 inside a glass-ceramic scaffold: a meso-macroporous system for acid catalysis. J Eur Ceram Soc 2013;33:1535-43.

[44] Zhang K, Wang Y, Hillmayer MA, Francis LF. Processing and properties of porous poly(L-lactide)/bioactive glass composites. Biomaterials 2004;25:2489-500.

[45] Baino F, Verné E, Vitale-Brovarone C. Feasibility, tailoring and properties of polyurethane/bioactive glass composite scaffolds for tissue engineering. J Mater Sci: Mater Med 2009;20:2189-195.

[46] ASTM C633-01 (2008). Standard test method for adhesion or cohesion strength of thermal spray coatings.

[47] Gibson LJ, Ashby MF. Cellular solids: structure and properties. 2nd ed. Cambridge: Cambridge University Press; 1997.

[48] Doblaré M, Garca JM, Gómez MJ. Modelling bone tissue fracture and healing: a review. Eng Fract Mech 2004;71:1809-40.

[49] Chen Q, Baino F, Pugno NM, Vitale-Brovarone C. Bonding strength of glass-ceramic trabecular-like coatings to ceramic substrates for prosthetic applications. Mater Sci Eng C 2013;33:1530-8.

[50] Kendall K, Howard AJ, Birchall JD, Pratt PL, Proctor BA, Jefferis SA. The relation between porosity, microstructure and strength, and the approach to advanced cement-based materials [and discussion]. Phil Trans R Soc Lond A 1983;310:139-53.

[51] Rice RW. Grain size and porosity dependence of ceramic fracture energy and toughness at 22 °C. J Mater Sci 1996;31:1969-83.

[52] Sadowski T, Samborski S. Modeling of porous ceramics response to compressive loading. J Am Ceram Soc 2003;86:2218-21.

[53] Arnold M, Boccaccini AR, Ondracek G. Prediction of the Poisson's ratio of porous materials. J Mater Sci 1996;31:1643-6.

[54] Pugno N. The role of defects in the design of the space elevator cable: from a nano to a mega tube. Acta Mater 2007;55:5269-79.

[55] Irwin GR. Crack-extension force for a part-through crack in a plate. J Appl Mech 1962;29:651-4.

[56] Pugno N, Ruoff R. Quantized fracture mechanics. Phil Mag 2004;84:2829-45.

[57] Pugno N. Dynamic quantized fracture mechanics. Int J Fract 2006;140:159-68.

[58] Sack RA. Extension of Griffith's theory of rupture to three dimensions. Proc Phys Soc 1946;58:729-36.

[59] Keaveny TM, Morgan EF, Niebur GL, Yeh OC. Biomechanics of trabecular bone. Ann Rev Biomed Eng 2001;3:307-33.

[60] Keller TS. Predicting the compressive mechanical behavior of bone. J Biomech 1994;27:1159-68.

[61] Keyak JH, Lee I, Skinner HB. Correlations between orthogonal mechanical properties and density of trabecular bone: use of different densitometric measures. J Biomed Mater Res 1994;28:1329-36.

[62] Hench LL, Wilson J. An introduction to bioceramics. Singapore: World Scientific; 1993.

[63] Kaplan SJ, Hayes WC, Stone JL, Beaupré GS. Tensile strength of bovine trabecular bone. J Biomech 1985;18:723-7.

[64] Esen Z, Bor S. Characterization of Ti–6Al–4V alloy foams synthesized by space holder technique. Mater Sci Eng A 2011;528:3200–9.

[65] Rezwan K, Chen QZ, Blaker JJ, Boccaccini AR. Biodegradable and bioactive porous polymer/inorganic composite scaffolds for bone tissue engineering. Biomaterials 2006;27:3413-31

[66] Karageorgiou V, Kaplan D. Porosity of 3D biomaterial scaffolds and osteogenesis. Biomaterials 2005;26:5474-91.

Figure legends

Fig. 1. Linear relationships between porosity and compressive strength of bioactive glass-ceramic scaffolds for hard-tissue engineering (picture adapted from Gerhardt and Boccaccini [12]). The large variations of compressive strength values are due to different starting glass compositions and fabrication methods, resulting in different pore morphologies, pore sizes, pore size distributions as well as different shapes and thicknesses of the scaffold struts.

Fig. 2. Reference scheme for the development of the tensile model.

Fig. 3. Scaffolds fabrication: (a) starting open-cells PU sponge (magnification 100×); (b) glass-coated polymer before the high-temperature thermal treatment (magnification 150×).

Fig. 4. Sintered scaffolds: (a) BG32 scaffolds on a platinum plate just before the extraction from the sintering furnace (size of each sample about 10 mm × 10 mm × 10 mm); SEM micrographs of the porous architecture of (b) BG32 scaffolds (magnification 300×) (the white circles and arrows indicate the absence of inner cavities along the axis of the struts, which might have been originated by the starting PU template), (c) CEL2 scaffolds (magnification 200×) and (d) SCNA scaffolds (magnification 300×).

Fig. 5. Micro-CT analysis on the prepared scaffolds (left: 3-D reconstruction of the scaffold volume; right: mid-length cross-sections in the [xy], [xz] and [yz] orthogonal planes): (a) BG32 scaffold (porosity ~70 vol.%), (b) CEL2 scaffold (porosity ~61 vol.%) and (c) SCNA scaffold (porosity ~45 vol.%).

Fig. 6. Compressive case: comparison between experimental data and model results between (a) 45S5 Bioglass (BG5 and BG32) scaffolds, (b) CEL2 and SCNA scaffolds, (c) all scaffolds batches.

Fig. 7. Tensile case: comparison between experimental data and model results for SCNA scaffolds.

Tables

Table 1. Compositions and synthesis conditions of the starting glasses.

Glass	Composition (mol.%)							Raw products	Melting conditions
	SiO_2	P_2O_5	CaO	Na_2O	MgO	K_2O	Al_2O_3		
45S5 Bioglass	46.1	2.6	26.9	24.4	-	-	-	SiO_2, $Ca_3(PO_4)_2$, $CaCO_3$, Na_2CO_3	1,500 °C for 1 h (heating rate: 15 °C min^{-1})
CEL2	45.0	3.0	26.0	15.0	7.0	4.0	-	SiO_2, $Ca_3(PO_4)_2$, $CaCO_3$, Na_2CO_3, $(MgCO_3)_4{\cdot}Mg(OH)_2{\cdot}5H_2O$, K_2CO_3	1,500 °C for 1 h (heating rate: 15 °C min^{-1})
SCNA	57	-	34	6	-	-	3	SiO_2, $CaCO_3$, Na_2CO_3, Al_2O_3	1,550 °C for 1 h (heating rate: 15 °C min^{-1})

Table 2. Sintering conditions and crystalline phases developed upon the thermal treatment.

Starting material	Sintering parameters [a]	Crystalline phases	References
BG5	1100 °C for 3 h	$Na_2CaSi_2O_6$, $Na_2Ca_4(PO_4)_2SiO_4$	[21]
BG32	1180 °C for 3 h	$Na_2CaSi_2O_6$, $Na_2Ca_4(PO_4)_2SiO_4$	[21]
CEL2	1000 °C for 3 h	$Na_4Ca_4(Si_6O_{18})$, $Ca_2Mg(Si_2O_7)$	[19]
SCNA	1000 °C for 3 h	$CaSiO_3$	[43,49]

[a] Heating and cooling rates set at 5 and 10 °C min^{-1}, respectively, in all cases.

Table 3. Compressive models parameters and coefficients of determination for the different scaffolds.

Scaffold material	*C* (MPa)	α	R^2
BG5	497	4.58	0.95
BG32	259	4.36	0.97
CEL2	33	2.44	0.67
SCNA	50	1.44	0.76

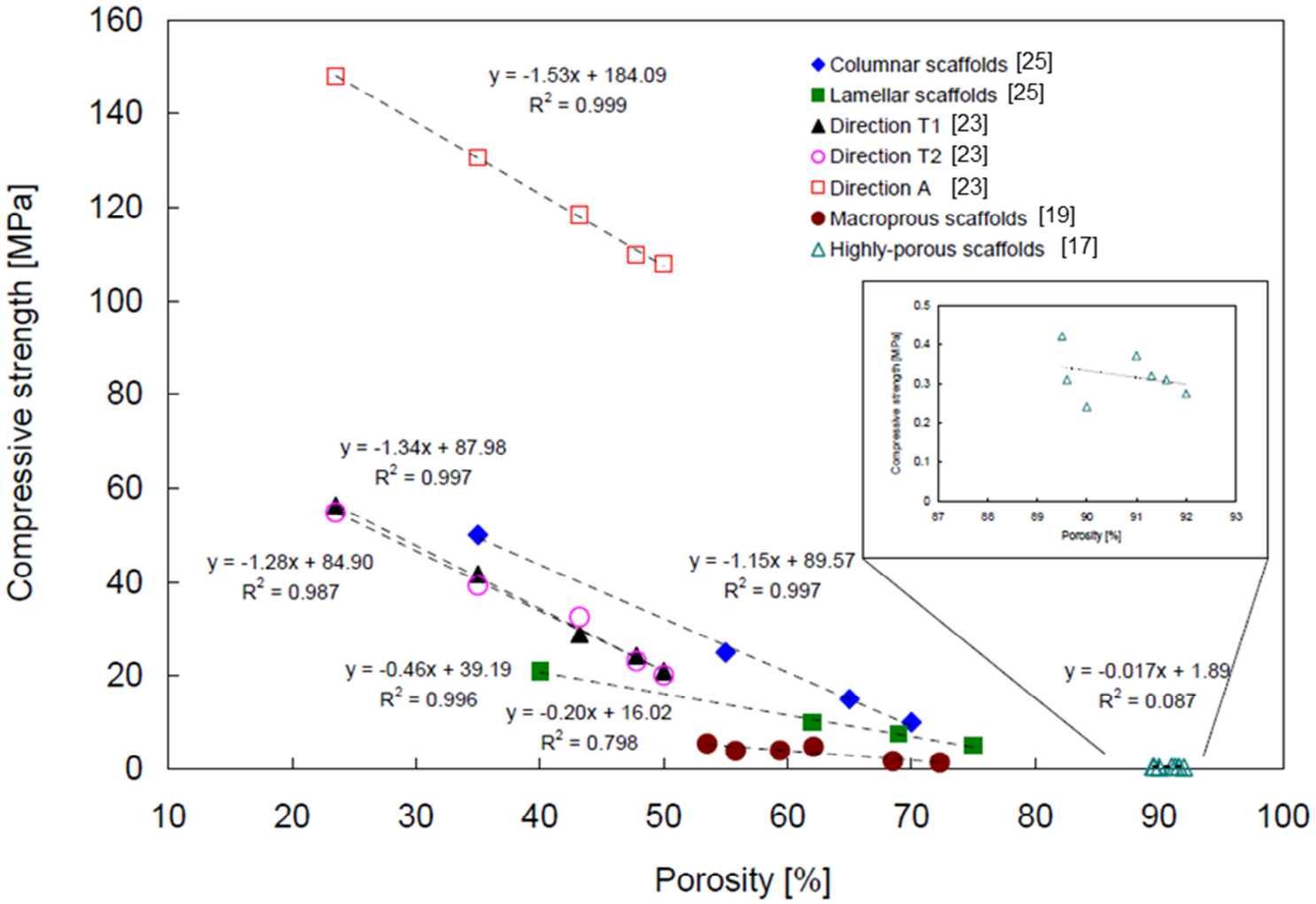
Compressive strength [MPa]
Porosity [%]
y = -1.53x + 184.09
R2 = 0.999
y = -1.34x + 87.98
R2 = 0.997
y = -1.28x + 84.90
R2 = 0.987
y = -1.15x + 89.57
R2 = 0.997
y = -0.46x + 39.19
R2 = 0.996
y = -0.20x + 16.02
R2 = 0.798
y = -0.017x + 1.89
R2 = 0.087
Columnar scaffolds [25]
Lamellar scaffolds [25]
Direction T1 [23]
Direction T2 [23]
Direction A [23]
Macroprous scaffolds [19]
Highly-porous scaffolds [17]

Fig. 1

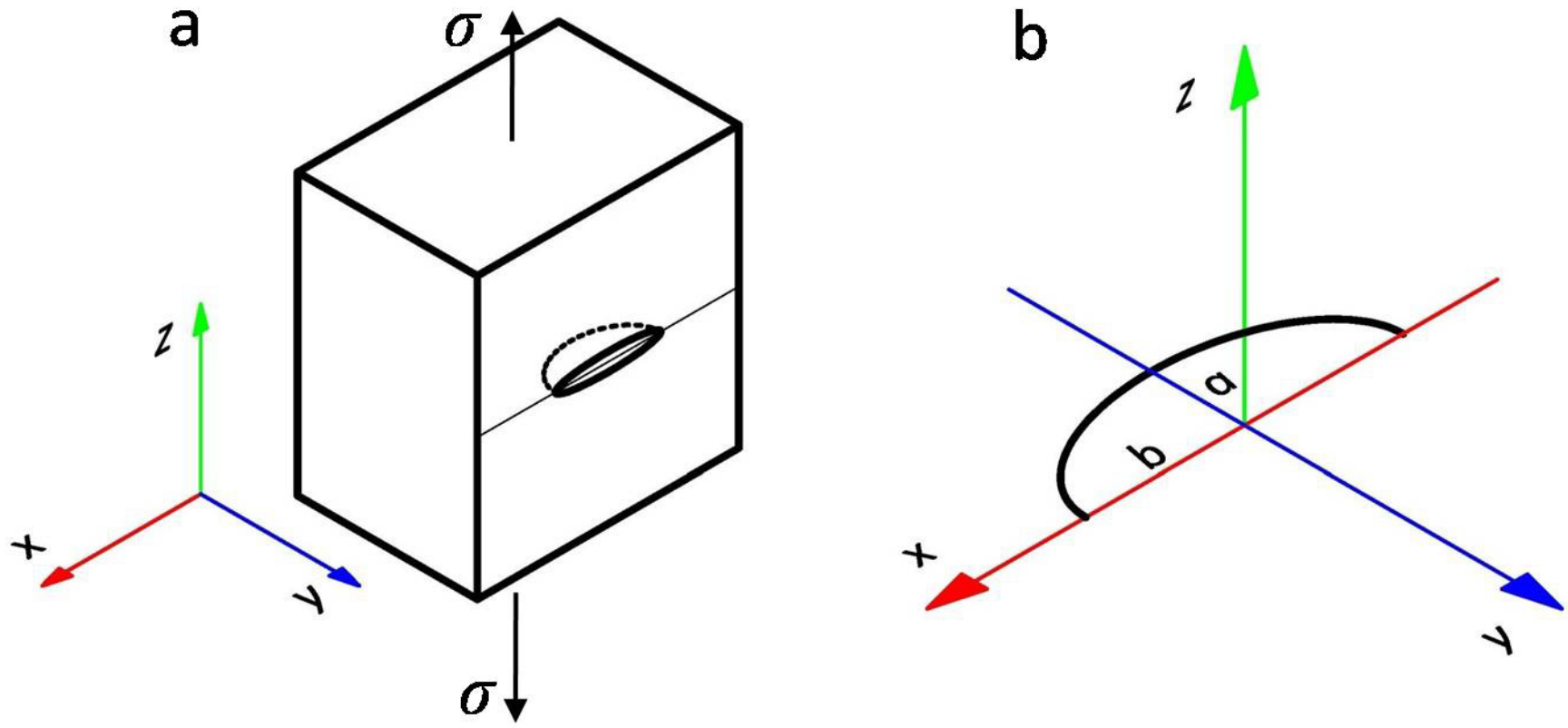

Fig. 2

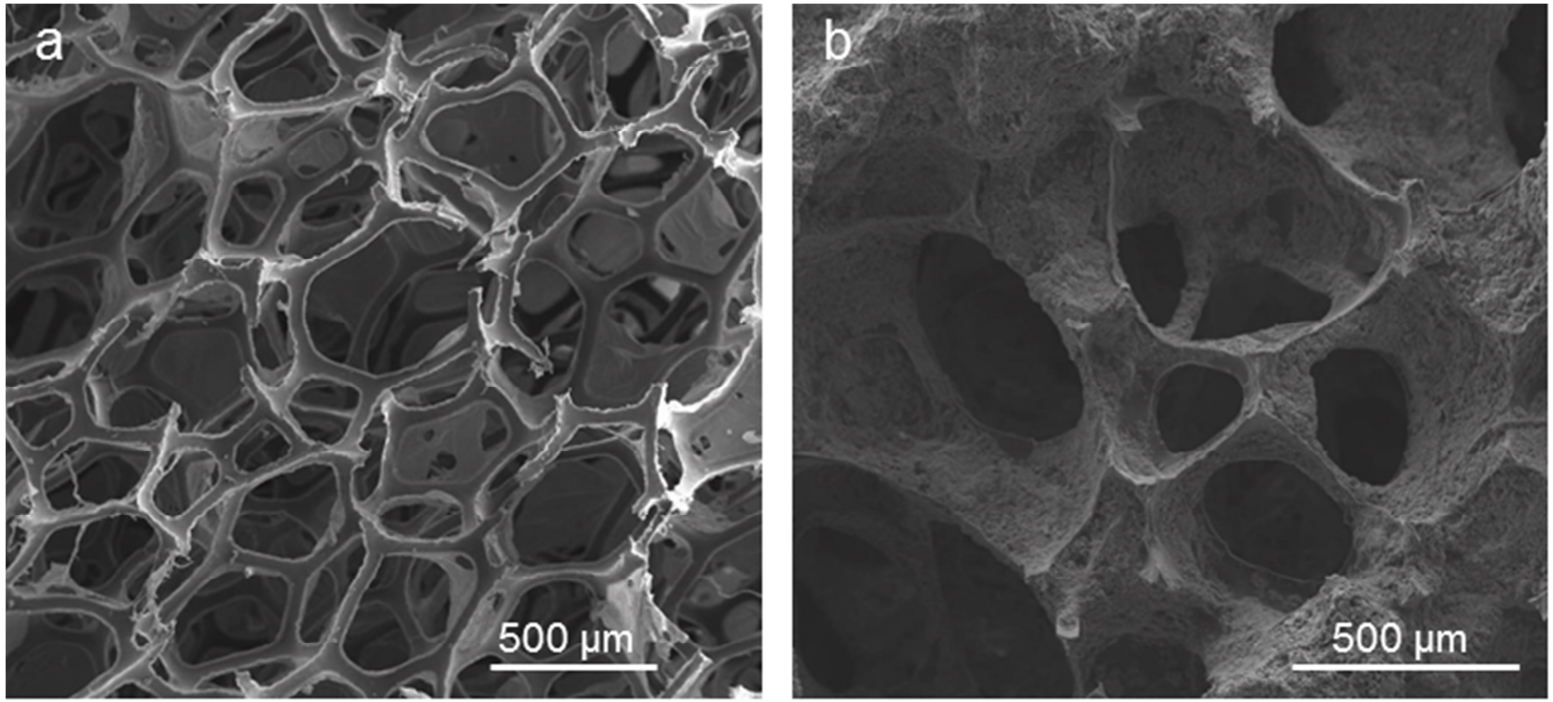

Fig,. 3

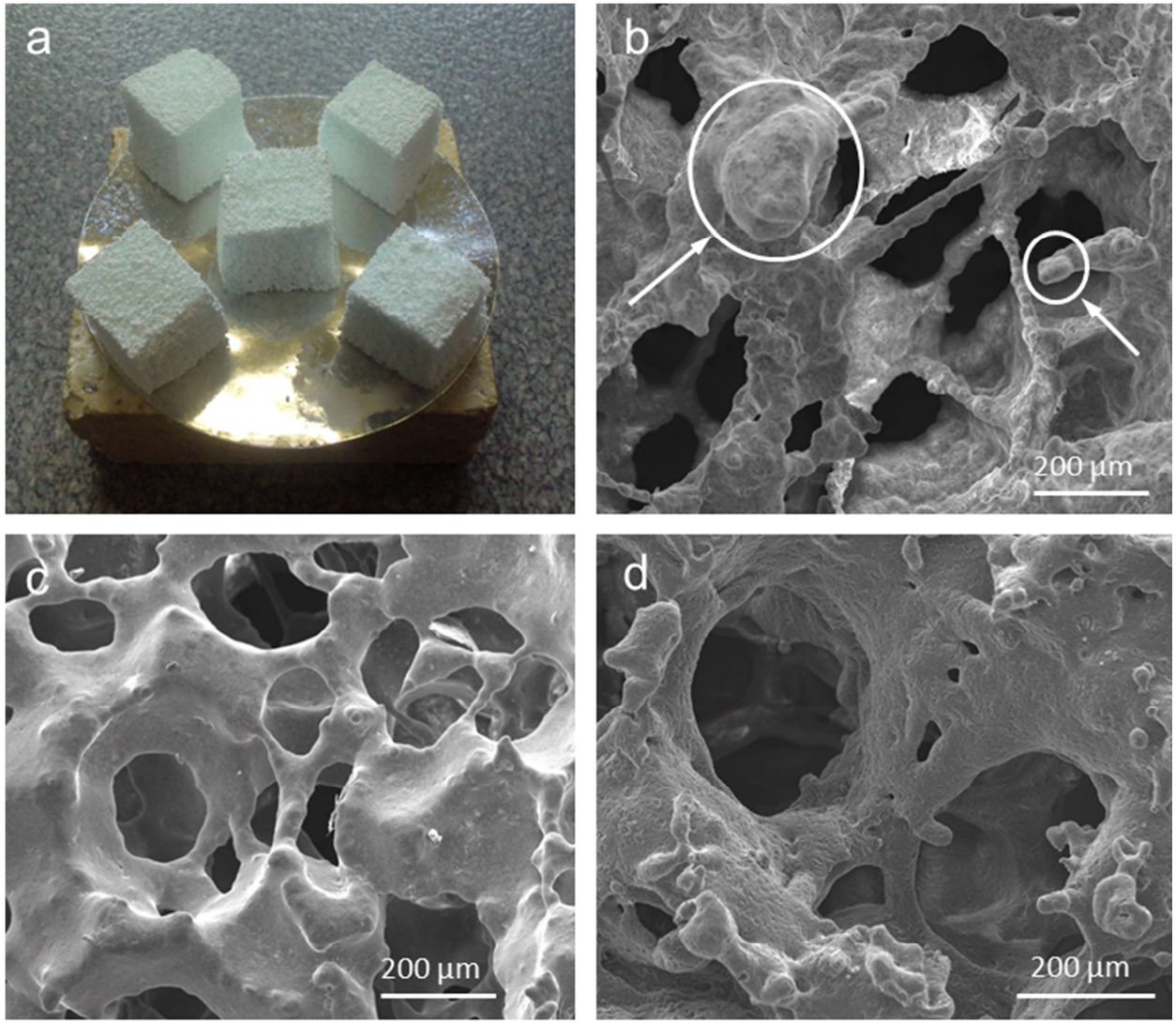

Fig. 4

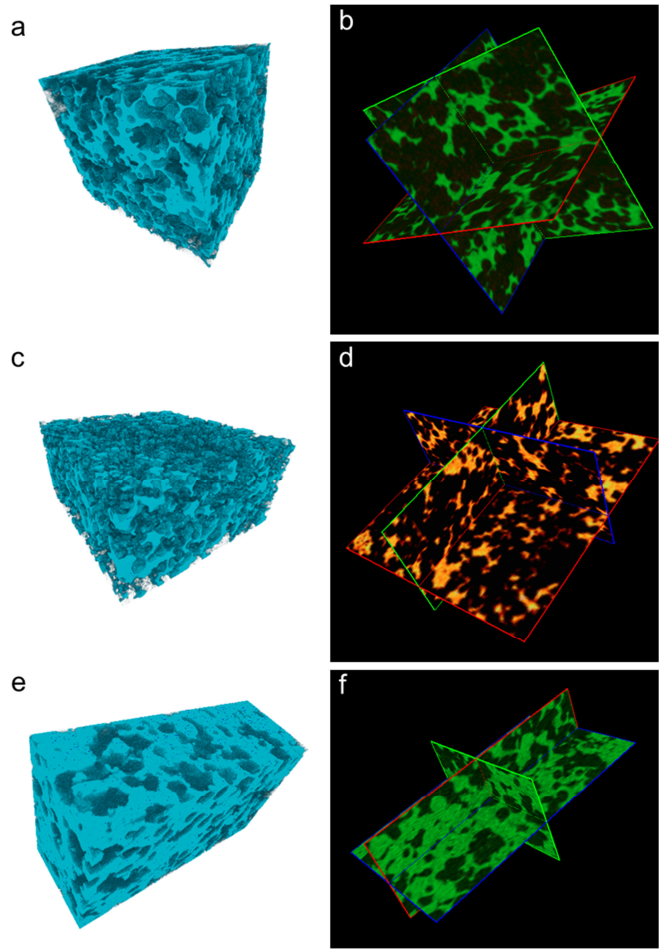

Fig. 5

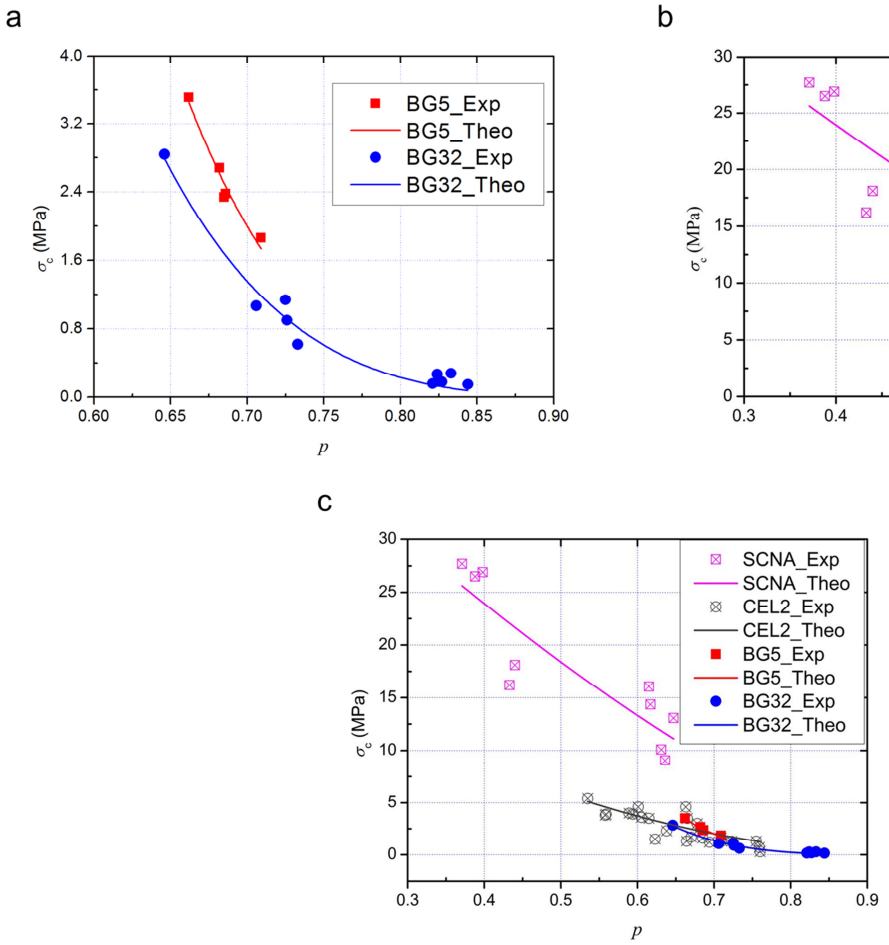
a
BG5_Exp
BG5_Theo
BG32_Exp
BG32_Theo
σ_c (MPa)
p
b
SCNA_Exp
SCNA_Theo
CEL2_Exp
CEL2_Theo
σ_c (MPa)
p
c
SCNA_Exp
SCNA_Theo
CEL2_Exp
CEL2_Theo
BG5_Exp
BG5_Theo
BG32_Exp
BG32_Theo
σ_c (MPa)
p

Fig. 6

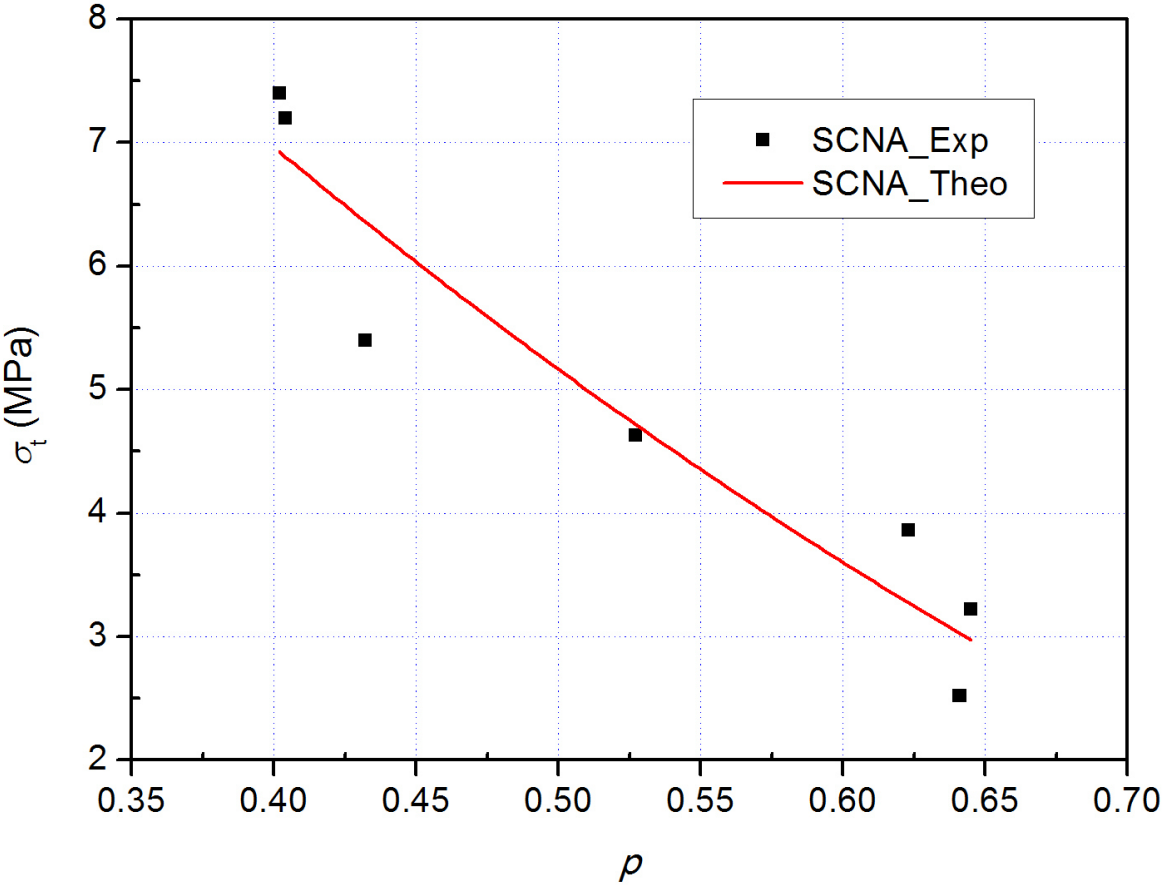
SCNA_Exp
SCNA_Theo
σ_t (MPa)
p
8
7
6
5
4
3
2
0.35
0.40
0.45
0.50
0.55
0.60
0.65
0.70

Fig. 7